3

MODELLING OF LOSSY MICROSTRIP LINES WITH FINITE THICKNESS

J. F. Kiang, S. M. Ali, and J. A. Kong

3.1 Introduction

For microwave integrated circuit applications, the characteristics of interconnects have been investigated for propagation modes [1,2], time response [3], crosstalk [4], coupling [5], delay [6], etc. In these analyses, it is assumed that quasi-TEM modes are guided along the multiconductor transmission line. In [1], the analysis was performed for two asymmetric transmission lines. In [2] and [3], an arbitrary number of transmission lines were analyzed. In [3], the load and the source conditions were presented in terms of the modal reflection and transmission coefficient matrices.

To perform the quasi-TEM analysis, the capacitance matrix for the multiconductor transmission line has to be obtained first. Both the spectral and the spatial domain methods have been proposed to

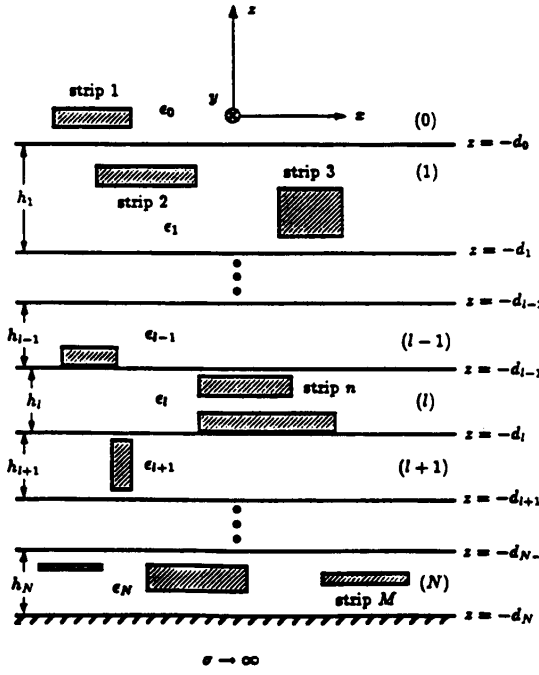

Figure 3.1 Geometrical configuration of M microstrip lines with finite thickness embedded in arbitrary layers of an isotropic stratified medium.

calculate the capacitance matrix. In the spectral domain methods, two side walls are used to enclose the whole transmission line structure, and the thickness of the strip lines has not been considered [7,8]. In using the spatial domain method [9], the structure has to be truncated to a finite extent to make the numerical implementation feasible. In [10], the infinite extent of the structure was incorporated, but only a two-layer medium was considered.

In practical microwave integrated circuits, the dielectric loss due to the substrate and the conductor loss due to the metallic strips have been studied in the analysis of circuit performances[11–13].

In this chapter, we present a quasi-TEM analysis of coupled lossy microstrip lines of finite strip thickness embedded in different layers of a lossy isotropic stratified medium as shown in Fig. 3.1. First, a spectral domain scalar Green's function in a lossy isotropic stratified medium is derived. In the formulation, no side walls are introduced, the transmission structure is not truncated, and the analysis is valid for arbitrary number of dielectric layers.

Based on the scalar Green's function, a set of coupled integral equations is obtained for the charge distribution on the strip surfaces. The method of moments is then applied where pulse basis functions and a point-matching scheme is used to solve numerically the set of integral equations for the charge distribution, and hence the capacitance matrix. The duality between the electrostatic formulation and the magnetostatic one is applied to calculate the inductance matrix. The conductance matrix is obtained by using the duality between the electrostatic problem and the current field problem. A perturbation method is used to calculate the resistance matrix.

Finally, a transmission line analysis is derived to obtain the transfer matrix for multiconductor line, which significantly reduces the effort in treating the load and the source conditions. Transient responses are obtained by using the Fourier transform. The results for two coupled lines are presented.

3.2 Integral Equation Formulation

We first formulate the scalar Green's function in the spectral domain in a homogeneous medium of permittivity ϵ with a ground plane located at $z = 0$. Thus, we consider a uniform line charge of unit amplitude to be located at (x', z') along the y direction, and evaluate the electrostatic potential at (x, z).

The scalar Green's function $g(\overline{r}, \overline{r}')$ is the solution of the following Poisson equation :

$$\nabla_s^2 g(\overline{r}, \overline{r}') = -\frac{1}{\epsilon}\delta(\overline{r} - \overline{r}') \tag{1}$$

where $\nabla_s^2 = \partial^2/\partial x^2 + \partial^2/\partial z^2$, $\overline{r} = \hat{x}x + \hat{z}z$, and $\overline{r}' = \hat{x}x' + \hat{z}z'$. The scalar Green's function can be expressed in the spectral domain as

$$g(\overline{r}, \overline{r}') = \iint_{-\infty}^{\infty} dk_x dk_z e^{ik_x x + ik_z z} \tilde{g}(\overline{k}_s) \tag{2}$$

where $\overline{k}_s = \hat{x}k_x + \hat{z}k_z$, and $\tilde{g}(\overline{k}_s)$ is the Fourier transform of $g(\overline{r}, \overline{r}')$ with respect to x and z. Substituting (2) into (1), and using the image theory, we get

$$\tilde{g}(\overline{k}_s) = \frac{1}{4\pi^2\epsilon(k_x^2 + k_z^2)}\left[e^{-ik_x x' - ik_z z'} - e^{-ik_x x' + ik_z z'}\right] \tag{3}$$

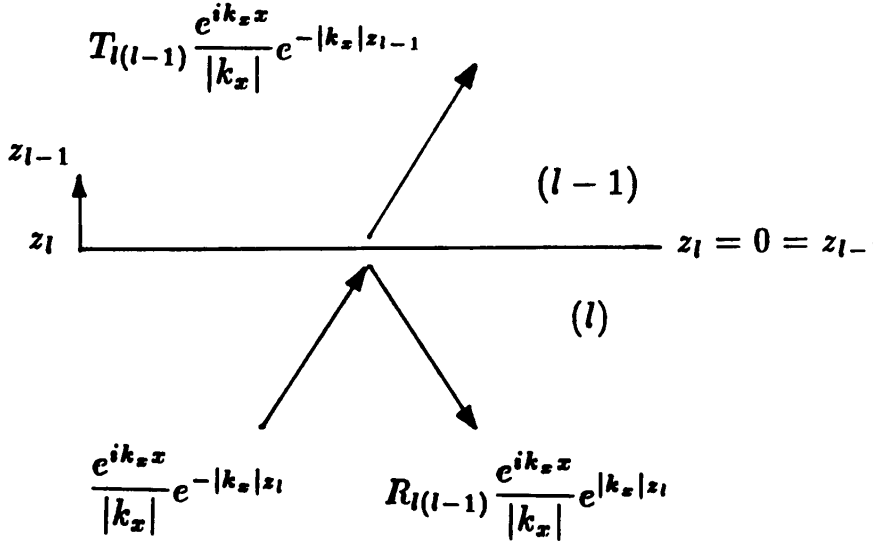

Figure 3.2 Definition of the local reflection and transmission coefficients at a dielectric interface between media (l) and $(l-1)$.

The second term is the Fourier transform of the Green's function due to the image line charge at $\bar{r}_I' = \hat{x}x' - \hat{z}z'$ which is the image of $\bar{r}'$ with respect to the ground plane at $z = 0$. The scalar Green's function can then be written as

$$g(\bar{r}, \bar{r}') = \iint_{-\infty}^{\infty} dk_x dk_z e^{ik_x(x-x')} \frac{e^{ik_z(z-z')} - e^{ik_z(z+z')}}{4\pi^2 \epsilon (k_x^2 + k_z^2)} \tag{4}$$

By contour integration in the complex k_z plane, we have

$$g(\bar{r}, \bar{r}') = \int_{-\infty}^{\infty} dk_x \frac{e^{ik_x(x-x')}}{4\pi\epsilon|k_x|} \left[e^{-|k_x||z-z'|} - e^{-|k_x|(z+z')} \right] \tag{5}$$

The integrand is regular at $k_x = 0$, and the integration is well defined as $\bar{r}$ goes to infinity.

Next, we introduce local reflection and transmission coefficients at a boundary between two dielectrics. Consider a dielectric interface between media (l) and $(l-1)$ as shown in Fig. 3.2. We assume that the spectral domain potential in each region can be expressed as

$$\phi_l(\bar{r}, k_x) = \frac{e^{ik_x x}}{|k_x|} \left[e^{-|k_x| z_l} + R_{l(l-1)} e^{|k_x| z_l} \right] \tag{6a}$$

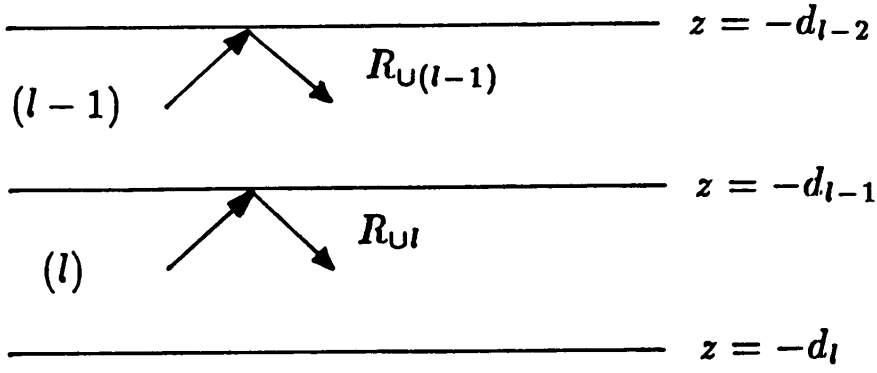

Figure 3.3 Definition of the global reflection coefficients at the upper boundaries of dielectric layers (l) and $(l-1)$.

$$\phi_{l-1}(\bar{r}, k_x) = \frac{e^{ik_x x}}{|k_x|} T_{l(l-1)} e^{-|k_x| z_{l-1}} \tag{6b}$$

where $z_l = z_{l-1} = z + d_{l-1}$, $R_{l(l-1)}$ and $T_{l(l-1)}$ are constants to be determined. The z component of the electric field in each region can be obtained as

$$E_{lz}(\bar{r}, k_x) = e^{ik_x x} \left[e^{-|k_x| z_l} - R_{l(l-1)} e^{|k_x| z_l} \right] \tag{7a}$$

$$E_{(l-1)z}(\bar{r}, k_x) = T_{l(l-1)} e^{ik_x x} e^{-|k_x| z_{l-1}} \tag{7b}$$

By imposing the boundary conditions that the potential and the normal component of the electric flux density are continuous at $z = -d_{l-1}$, we obtain

$$R_{l(l-1)} = \frac{\epsilon_l - \epsilon_{l-1}}{\epsilon_l + \epsilon_{l-1}} \tag{8a}$$

$$T_{l(l-1)} = \frac{2\epsilon_l}{\epsilon_l + \epsilon_{l-1}} \tag{8b}$$

where $R_{l(l-1)}$ and $T_{l(l-1)}$ can be interpreted as local reflection and transmission coefficients, respectively.

Next, consider the two source-free layers (l) and $(l-1)$ of the stratified medium as shown in Fig. 3.3, where the potential and the z

component of the electric field in each layer can be expressed as

$$\phi_j(\bar{r}, k_x) = \frac{e^{ik_x x}}{|k_x|}\left[A_j e^{-|k_x|z_j} + B_j e^{|k_x|z_j}\right] \tag{9a}$$

$$E_{jz}(\bar{r}, k_x) = e^{ik_x x}\left[A_j e^{-|k_x|z_j} - B_j e^{|k_x|z_j}\right] \tag{9b}$$

where $z_j = z + d_j$ and $j = l,\ l-1$. We introduce the global reflection coefficient $R_{\cup j}$ defined at the upper boundary of layer (j), $z = -d_{j-1}$, as

$$R_{\cup j} = \frac{B_j e^{|k_x|h_j}}{A_j e^{-|k_x|h_j}} \tag{10}$$

where h_j is the thickness of layer (j). By imposing the boundary conditions at $z = -d_{l-1}$, we obtain the following recursive relation

$$R_{\cup l} = \frac{R_{l(l-1)} + R_{\cup(l-1)}e^{-2|k_x|h_{l-1}}}{1 + R_{l(l-1)}R_{\cup(l-1)}e^{-2|k_x|h_{l-1}}}, \qquad l = 2, \cdots, N \tag{11}$$

and $R_{\cup 1} = R_{10}$. Similarly, the global reflection coefficient $R_{\cap j}$ is defined at the lower boundary of layer (j), $z = -d_j$, as

$$R_{\cap j} = \frac{A_j}{B_j}. \tag{12}$$

By imposing the boundary condition at $z = -d_l$, we obtain

$$R_{\cap l} = \frac{R_{l(l+1)} + R_{\cap(l+1)}e^{-2|k_x|h_{l+1}}}{1 + R_{l(l+1)}R_{\cap(l+1)}e^{-2|k_x|h_{l+1}}}, \qquad l = N-1, \cdots, 0 \tag{13}$$

and $R_{\cap N} = -1$.

With the use of the above reflection coefficients, the expression of the scalar Green's function in a layered medium can be obtained in a simple way. For the case where both the line charge and the observation point are located in the upper half-space, that is layer (0), we have

$$g_{00}(\bar{r}, \bar{r}') = \frac{1}{4\pi\epsilon_0}\int_{-\infty}^{\infty} dk_x \frac{e^{ik_x(x-x')}}{|k_x|} \left[e^{-|k_x||z_0 - z_0'|} + R_{\cap 0}e^{-|k_x|(z_0+z_0')}\right] \tag{14}$$

where $z_0 = z + d_0$, $z_0' = z' + d_0$, the uniform line charge of unit amplitude is located at $\bar{r}' = (x', z_0')$, and the observation point is located at $\bar{r} = (x, z_0)$. The first term inside the brackets is the direct term, and the second term can be interpreted as due to the reflection from the lower boundary at $z = -d_0$.

For the case when both the line charge and the observation point are both located in an arbitrary layer (l) with $l \neq 0$, the Green's function can be expressed as

$$g_{ll}(\bar{r}, \bar{r}') = \frac{1}{4\pi\epsilon_l} \int_{-\infty}^{\infty} dk_x \frac{e^{ik_x(x-x')}}{|k_x|} \left[e^{-|k_x||z_l - z_l'|} + A(k_x) e^{-|k_x| z_l} + B(k_x) e^{|k_x| z_l} \right] \tag{15}$$

where $z_l = z + d_l$, $z_l' = z' + d_l$, $A(k_x)$ and $B(k_x)$ are the unknowns to be determined. From the definition of $R_{\cup l}$ and $R_{\cap l}$, we have

$$R_{\cup l}\left[e^{-|k_x|(z_l - z_l')} + A(k_x) e^{-|k_x| z_l} \right] = B(k_x) e^{|k_x| z_l}, \quad z_l = h_l \tag{16a}$$

$$R_{\cap l}\left[e^{-|k_x|(z_l' - z_l)} + B(k_x) e^{|k_x| z_l} \right] = A(k_x) e^{-|k_x| z_l}, \quad z_l = 0 \tag{16b}$$

By solving (16), we get

$$A(k_x) = \frac{R_{\cap l} e^{-|k_x| z_l'} + R_{\cup l} R_{\cap l} e^{-|k_x|(2h_l - z_l')}}{1 - R_{\cup l} R_{\cap l} e^{-2|k_x| h_l}} \tag{17a}$$

$$B(k_x) = \frac{R_{\cup l} e^{-|k_x|(2h_l - z_l')} + R_{\cup l} R_{\cap l} e^{-|k_x|(2h_l + z_l')}}{1 - R_{\cup l} R_{\cap l} e^{-2|k_x| h_l}} \tag{17b}$$

Substituting (17) into (15), we obtain the explicit form of the Green's function $g_{ll}(\bar{r}, \bar{r}')$ in the layer (l) as

$$g_{ll}(\bar{r}, \bar{r}') = \frac{1}{4\pi\epsilon_l} \int_{-\infty}^{\infty} dk_x \frac{e^{ik_x(x-x')}}{|k_x|} \left\{ e^{-|k_x||z_l - z_l'|} + \frac{1}{1 - R_{\cup l} R_{\cap l} e^{-2|k_x| h_l}} \left[R_{\cup l} e^{-|k_x|(2h_l - z_l - z_l')} + R_{\cap l} e^{-|k_x|(z_l + z_l')} + R_{\cup l} R_{\cap l} e^{-|k_x|(z_l - z_l' + 2h_l)} + R_{\cup l} R_{\cap l} e^{-|k_x|(-z_l + z_l' + 2h_l)} \right] \right\} \tag{18}$$

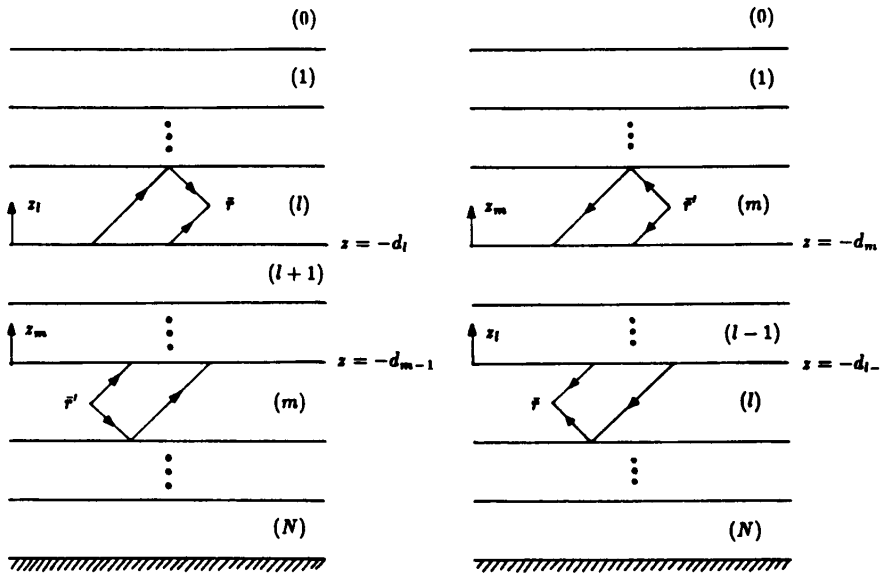

Figure 3.4 Determination of the scalar Green's function where the source is in a layer (m) and the observation point is in the layer (l). (a) Layer (l) is above layer (m). (b) Layer (l) is below layer (m).

The first term inside the brace is the direct term, the other terms are the summation of the multiple reflections between the two boundaries at $z = -d_{l-1}$ and $z = -d_l$. It is observed that (14) is a special case of (18) with $l = 0$ and $R_{Ul} = 0$.

Next, we consider the case when the source and the observation points are in different layers. As shown in Fig. 3.4(a), the source is in a layer (m) and the observation point is in a layer (l) which is above layer (m). We assume that each spectral field component is transmitted upward from the source layer (m) to the layer (l) with the upward transmission coefficient $X_{Ul,m}$. The Green's function can thus be expressed as

$$g_{lm}(\bar{r}_>, \bar{r}'_<) = \frac{1}{4\pi\epsilon_m} \int_{-\infty}^{\infty} dk_x \frac{e^{ik_x(x-x')}}{|k_x|} X_{Ul,m} \left[e^{-|k_\rho| z_l} + R_{Ul} e^{-|k_\rho|(2h_l - z_l)} \right] \frac{e^{|k_\rho| z'_m} + R_{\cap m} e^{-|k_\rho|(2h_m + z'_m)}}{1 - R_{Um} R_{\cap m} e^{-2|k_\rho| h_m}} \tag{19}$$

where z_l and z'_m are the local coordinates defined as $z_l = z + d_l$ and $z'_m = z' + d_{m-1}$, respectively. Similarly, when the observation point is located in the layer $(l+1)$, we have

$$g_{(l+1)m}(\overline{r}_>, \overline{r}'_<) = \frac{1}{4\pi\epsilon_m} \int_{-\infty}^{\infty} dk_x \frac{e^{ik_x(x-x')}}{|k_x|} X_{\cup(l+1),m} \left[e^{-|k_z|z_{l+1}} + R_{\cup(l+1)} e^{-|k_z|(2h_{l+1}-z_{l+1})}\right] \frac{e^{|k_z|z'_m} + R_{\cap m} e^{-|k_z|(2h_m+z'_m)}}{1 - R_{\cup m} R_{\cap m} e^{-2|k_z|h_m}} \tag{20}$$

where $z_{l+1} = z + d_{l+1}$. Imposing the boundary conditions at the interface $z = -d_l$, we get

$$X_{\cup l,m} = X_{\cup(l+1),m} e^{-|k_z|h_{l+1}} \frac{1 + R_{\cup(l+1)}}{1 + R_{\cup l} e^{-2|k_z|h_l}}, \qquad l = m-2, \cdots, 0 \tag{21}$$

and for $l = m-1$, we have

$$X_{\cup(m-1),m} = \frac{1 + R_{\cup m}}{1 + R_{\cup(m-1)} e^{-2|k_z|h_{m-1}}} \tag{22}$$

For the case when the layer (m) is above layer (l) as shown in Fig. 3.4(b), the Green's function may be expressed as

$$g_{lm}(\overline{r}_<, \overline{r}'_>) = \frac{1}{4\pi\epsilon_m} \int_{-\infty}^{\infty} dk_x \frac{e^{ik_x(x-x')}}{|k_x|} X_{\cap l,m} \left[e^{|k_z|z_l} + R_{\cap l} e^{-|k_z|(2h_l+z_l)}\right] \frac{e^{-|k_z|z'_m} + R_{\cup m} e^{-|k_z|(2h_m-z'_m)}}{1 - R_{\cup m} R_{\cap m} e^{-2|k_z|h_m}} \tag{23}$$

where $X_{\cap l,m}$ is the downward transmission coefficient, z_l and z'_m are the local coordinates defined as $z_l = z + d_{l-1}$ and $z'_m = z' + d_m$, respectively. Similarly, when the observation point is located in the layer $(l-1)$, we have

$$g_{(l-1)m}(\overline{r}_<, \overline{r}'_>) = \frac{1}{4\pi\epsilon_m} \int_{-\infty}^{\infty} dk_x \frac{e^{ik_x(x-x')}}{|k_x|} X_{\cap(l-1),m} \left[e^{|k_z|z_{l-1}} + R_{\cap(l-1)} e^{-|k_z|(2h_{l-1}+z_{l-1})}\right] \frac{e^{-|k_z|z'_m} + R_{\cup m} e^{-|k_z|(2h_m-z'_m)}}{1 - R_{\cup m} R_{\cap m} e^{-2|k_z|h_m}} \tag{24}$$

where $z_{l-1} = z + d_{l-2}$. Imposing the boundary conditions at the interface $z = -d_{l-1}$, we have

$$X_{\cap l,m} = X_{\cap(l-1),m} e^{-|k_\rho| h_{l-1}} \frac{1 + R_{\cap(l-1)}}{1 + R_{\cap l} e^{-2|k_\rho| h_l}}, \qquad l = m+2, \cdots, N \tag{25}$$

and for $l = m+1$, we have

$$X_{\cap(m+1),m} = \frac{1 + R_{\cap m}}{1 + R_{\cap(m+1)} e^{-2|k_\rho| h_{m+1}}} \tag{26}$$

Next, consider M microstrip lines embedded in arbitrary layers of an isotropic stratified medium as shown in Fig. 3.1. All the conductor strips are of finite thickness, the permittivity of layer (j) is ϵ_j, and a ground plane is put at $z = -d_N$ as the potential reference.

Using the scalar Green's function, the potential in layer (l) can be represented as

$$V_l(\bar{r}) = \sum_{p=1}^{M} \int_{\Gamma_p} d\bar{r}' g_{lL(p)}(\bar{r}, \bar{r}') \rho_p(\bar{r}') \tag{27}$$

where Γ_p is the cross section contour of the pth microstrip line, $\rho_p(\bar{r}')$ is the charge density on the pth microstrip surface, $L(p)$ is the layer where the pth microstrip line is embedded. The cross section of the microstrip lines can be arbitrary in general. For practical applications, only the rectangular cross sections are considered.

The potential distribution in (27) satisfies all the boundary conditions that the potential and the normal electric flux density are continuous across the interfaces between adjacent dielectric layers. To obtain the charge distribution on each microstrip surface, we impose the boundary condition that the potential on each microstrip is equal to the impressed voltage. Thus we have

$$\sum_{p=1}^{M} \int_{\Gamma_p} d\bar{r}' g_{L(q)L(p)}(\bar{r}, \bar{r}') \rho_p(\bar{r}') = V_q, \qquad \bar{r} \text{ on } \Gamma_q \tag{28}$$

where $q = 1, \cdots, M$.

In the next section, the method of moments is applied to solve (28) for the charge distributions.

3.3 Numerical Solution of Charge Distribution

By applying the method of moments to solve (28), we first choose a set of pulse basis functions for the surface charge density, hence

$$\rho_p(\overline{r}') = \sum_{i=1}^{N_p} a_{pi} P_{pi}(\overline{r}'), \qquad p = 1, \cdots, M \tag{29}$$

where a_{pi} and $P_{pi}(\overline{r}')$ are, respectively, the expansion coefficients and the basis functions on the ith section of the pth microstrip surface; and N_p is the total number of basis functions on the pth microstrip surface. The pulse function is defined as

$$P_{pi}(\overline{r}) = \begin{cases} 1, & \overline{r} \text{ on } \Gamma_{pi} \\ 0, & \text{elsewhere} \end{cases} \tag{30}$$

where Γ_{pi} is the ith section on the pth microstrip surface.

Substituting (29) into (28), we have

$$\sum_{p=1}^{M} \sum_{i=1}^{N_p} a_{pi} \int_{\Gamma_{pi}} d\overline{r}' g_{L(q)L(p)}(\overline{r}, \overline{r}') P_{pi}(\overline{r}') = V_q, \qquad \overline{r} \text{ on } \Gamma_q \tag{31}$$

where $q = 1, \cdots, M$.

Next, we choose the center point at each pulse basis as the testing point to test (31), thus we have

$$\sum_{p=1}^{M} \sum_{i=1}^{N_p} Z_{qj,pi} a_{pi} = \beta_{qj}, \qquad 1 \le q \le M, 1 \le j \le N_q \tag{32}$$

where

$$Z_{qj,pi} = \int_{\Gamma_{pi}} d\overline{r}' g_{L(q)L(p)}(\overline{r}_{qj}, \overline{r}') P_{pi}(\overline{r}') \tag{33}$$

$$\beta_{qj} = V_q \tag{34}$$

and $\overline{r}_{qj} = (x_{qj}, z_{qj})$ is the center coordinate of Γ_{qj}. By solving (32) for a_{pi}'s, the charge density can be obtained.

The capacitance matrix $\overline{\overline{C}}$ of M microstrip lines can be obtained by solving (28) M times. For the nth time, all the microstrip lines are

grounded except that one volt is imposed on the n th line. By solving (32), the charge distribution is obtained. The total surface charge per unit length on the m th microstrip line is equal to the mn th element of the capacitance matrix, C_{mn} . This can be observed from the definition of the capacitance matrix

$$\sum_{p=1}^{M} C_{qp} V_p = Q_q, \qquad 1 \leq q \leq M \tag{35}$$

By setting $V_p = \delta_{p,n}$, we have $Q_q^{(n)} = C_{qn}$ with $1 \leq q \leq M$. Here, $\delta_{p,n}$ is the Kronecker's delta function and the superscript (n) in $Q_q^{(n)}$ is the index of the microstrip where one volt is imposed.

3.4 Magnetostatic Dual Problem

In this section, we briefly review the magnetostatic dual problem. For nonmagnetic materials, the magnetostatic problem for the geometrical configuration shown in Fig. 3.1 is equivalent to the one where all the dielectric media are replaced by the free space. The magnetostatic potential $\psi(\overline{r})$ due to a uniform line current at $\overline{r}'$ can be derived in a way similar to that in Section 2 as

$$\sum_{p=1}^{M} \int_{\Gamma_p} ds' g^M_{L(q)L(p)}(\overline{r}, \overline{r}') J_p(\overline{r}') = \psi_q, \qquad \overline{r} \text{ on } \Gamma_q \tag{36}$$

where $q = 1, \cdots, M$; $g^M_{L(q)L(p)}(\overline{r}, \overline{r}')$ is the scalar Green's function; $J_p(\overline{r}')$ is the surface current on the p th microstrip surface; and ψ_q is the magnetostatic potential measured on the q th microstrip surface with respect to the ground plane, which is equal to the magnetic flux linkage between the q th microstrip line and the ground plane per unit length.

Instead of solving (36) directly, a dual electrostatic problem for the same geometrical configuration in free space is solved. It can be shown that

$$g^M(\overline{r}, \overline{r}') = \mu_0 \epsilon_0 g^E(\overline{r}, \overline{r}') \tag{37}$$

where $g^E(\overline{r}, \overline{r}')$ is the scalar Green's function derived in Section 2 with all ϵ_l 's replaced by the dielectric constant in the free space.

Imposing the same boundary conditions that $V_q = \psi_q$ for $1 \leq q \leq M$, we have

$$J_p^{(k)}(\bar{r}) = \frac{\rho_P^{(k)}(\bar{r})}{\mu_0 \epsilon_0}, \qquad 1 \leq p, k \leq M \tag{38}$$

where $\rho_p^{(k)}(\bar{r})$ is the surface charge distribution on the pth microstrip surface when we impose one volt on the kth strip, and zero volt on the other strips; $J_p^{(k)}(\bar{r})$ is the surface current distribution on the pth microstrip surface when we impose one tesla-m on the kth strip, and zero tesla-m on the other strips.

In general, the surface current on the pth microstrip surface can be expressed as

$$J_p(\bar{r}) = \sum_{k=1}^{M} \psi_k J_p^{(k)}(\bar{r}) = \frac{1}{\mu_0 \epsilon_0} \sum_{k=1}^{M} \psi_k \rho_p^{(k)}(\bar{r}) \tag{39}$$

Integrating (39) over one unit length on the pth microstrip surface, we have

$$I_p = \frac{1}{\mu_0 \epsilon_0} \sum_{k=1}^{M} C_{0,pk} \psi_k \tag{40}$$

where I_p is the surface current on the pth microstrip line, and $C_{0,pk}$ is the pkth element of the capacitance matrix $\overline{\overline{C}}_0$ with all the dielectrics replaced by free space. Hence, we obtain the conventional result that the inductance matrix $\overline{\overline{L}}$ is proportional to the inverse of the capacitance matrix in free space as

$$\overline{\overline{L}} = \mu_0 \epsilon_0 \overline{\overline{C}}_0^{-1} \tag{41}$$

3.5 Calculation of $\overline{\overline{G}}$ and $\overline{\overline{R}}$

In this section, the dielectric loss and conductor loss are considered. The transmission line equations for M coupled microstrip lines are

$$-\frac{\partial \bar{I}}{\partial y} = \left[\overline{\overline{G}} - i\omega \overline{\overline{C}}\right] \cdot \bar{V} \tag{42a}$$

$$-\frac{\partial \bar{V}}{\partial y} = \left[\overline{\overline{R}} - i\omega \overline{\overline{L}}\right] \cdot \bar{I} \tag{42b}$$

where the conductance matrix $\overline{\overline{G}}$ accounts for the dielectric loss, and the resistance matrix $\overline{\overline{R}}$ accounts for the conductor loss.

The n th eigen solution to (42) can be represented as

$$\overline{I} = \overline{I}_n e^{-\gamma_n y} \tag{43a}$$

$$\overline{V} = \overline{V}_n e^{-\gamma_n y} \tag{43b}$$

where γ_n is the eigenvalue of the n th mode; and $\overline{I}_n$ and $\overline{V}_n$ are the corresponding eigenvectors. Substituting (43) into (42), we have

$$\gamma_n \overline{I}_n = \left[\overline{\overline{G}} - i\omega\overline{\overline{C}}\right] \cdot \overline{V}_n \tag{44a}$$

$$\gamma_n \overline{V}_n = \left[\overline{\overline{R}} - i\omega\overline{\overline{L}}\right] \cdot \overline{I}_n \tag{44b}$$

and hence

$$\gamma_n^2 \overline{I}_n = \left[\overline{\overline{G}} - i\omega\overline{\overline{C}}\right] \cdot \left[\overline{\overline{R}} - i\omega\overline{\overline{L}}\right] \cdot \overline{I}_n \tag{45a}$$

$$\gamma_n^2 \overline{V}_n = \left[\overline{\overline{R}} - i\omega\overline{\overline{L}}\right] \cdot \left[\overline{\overline{G}} - i\omega\overline{\overline{C}}\right] \cdot \overline{V}_n \tag{45b}$$

There are in general M eigen solutions to the above equations. The eigenvalues solved from (45a) and (45b) are the same; and the eigenvectors $\overline{I}_n$'s and $\overline{V}_n$'s are related by (44).

For the n th eigenmode, the time-average Poynting's power P_{nT} can be represented as

$$P_{nT} = \frac{1}{2}\mathrm{Re}\left[\overline{I}_n^{\dagger} \cdot \overline{V}_n\right] \tag{46}$$

where $\overline{I}_n^{\dagger}$ is the transposed, complex conjugate of $\overline{I}_n$. The time-average power loss per unit length P_{nL} along the transmission lines can be calculated as

$$P_{nL} = P_{nC} + P_{nD} = 2\alpha_{nT} P_{nT} \tag{47}$$

where

$$P_{nC} = (1/2)\overline{I}_n^{\dagger} \cdot \overline{\overline{R}} \cdot \overline{I}_n = 2\alpha_{nC} P_{nT} \tag{48a}$$

$$P_{nD} = (1/2)\overline{V}_n^{\dagger} \cdot \overline{\overline{G}} \cdot \overline{V}_n = 2\alpha_{nD} P_{nT} \tag{48b}$$

where P_{nC} and P_{nD} are the time-average conductor loss and dielectric loss per unit length, respectively; α_{nT}, α_{nC}, and α_{nD} are the corresponding attenuation constants for the n th mode.

To calculate the conductance matrix which accounts for the dielectric loss, we make use of the duality between the electrostatic problem and the current field problem. Assume that the geometrical configuration of the current field problem is the same as in Fig. 3.1, and the conductivity in layer (l) is designated by σ_l with $0 \leq l \leq N$. If the conductivities in the current field problem and the dielectric constants in the electrostatic problem satisfy the following relation

$$\frac{\sigma_0}{\epsilon_0} = \frac{\sigma_1}{\epsilon_1} = \cdots = \frac{\sigma_N}{\epsilon_N} = \alpha \tag{49}$$

then, we have

$$\overline{\overline{G}} = \alpha \overline{\overline{C}} \tag{50}$$

The perturbation method is used to solve for the attenuation constants α_{nC} and the resistance matrix $\overline{\overline{R}}$. We start from the lossless eigenvalue equations :

$$\begin{aligned} \overline{\overline{C}} \cdot \overline{\overline{L}} \cdot \overline{I}_{0n} &= \frac{1}{v_n^2} \overline{I}_{0n} \\ \overline{\overline{L}} \cdot \overline{\overline{C}} \cdot \overline{V}_{0n} &= \frac{1}{v_n^2} \overline{V}_{0n} \end{aligned} \tag{51}$$

where $\gamma_n = -i\beta_n$; $v_n = \omega/\beta_n$ is the phase velocity for the n th mode; and $\overline{\overline{C}}$ is the capacitance matrix with all materials lossfree. The time-average guided power can be approximated by the power guided along lossless lines as

$$P_{nT} \approx \frac{1}{2} \mathrm{Re}\left[\overline{I}_{0n}^{\dagger} \cdot \overline{V}_{0n}\right] \tag{52}$$

The power loss per unit length of the n th mode due to imperfect conductor can be calculated by using the surface current obtained for the perfect conductor lines. Thus, we have

$$P_{nC} = \frac{1}{2} \sum_{k=1}^{M'} R_{kS} \int_{\Gamma_k} |J_{nk}(\overline{r})|^2 \, d\overline{r} \tag{53}$$

where R_{kS} is the surface resistance per unit area on the k th microstrip surface, $J_{nk}(\overline{r})$ is the surface current distribution of the n th

mode on the k th microstrip surface. Here M' is the total number of conductors including the ground planes. As defined in (29), $\rho_k^{(i)}(\bar{r})$ can be expanded in terms of the pulse basis functions as

$$\rho_k^{(i)}(\bar{r}) = \sum_{m=1}^{N_k} a_{km}^{(i)} P_{km}(\bar{r}) \tag{54}$$

where $P_{km}(\bar{r})$ is the basis function defined in (30). By using (39), the surface current on the k th microstrip surface can be represented as

$$J_k(\bar{r}) = \frac{1}{\mu_0 \epsilon_0} \sum_{i=1}^{M} \psi_i \sum_{m=1}^{N_k} a_{km}^{(i)} P_{km}(\bar{r}) \tag{55}$$

where ψ_i is obtained by solving

$$\psi_i = \sum_{j=1}^{M} L_{ij} I_{0n,j} \tag{56}$$

where L_{ij} is the ij th element of the inductance matrix $\overline{\overline{L}}$, $I_{0n,j}$ is the j th element of the eigenvector $\bar{I}_{0n}$. The conductor loss can then be calculated as

$$P_{nC} = \frac{1}{2} \sum_{k=1}^{M} R_{kS} (\mu_0 \epsilon_0)^{-2} \sum_{m=1}^{N_k} \left| \sum_{i=1}^{M} \psi_i a_{km}^{(i)} \right|^2 \int_{\Gamma_{km}} |P_{km}(\bar{r})|^2 \, d\bar{r} + P_G \tag{57}$$

where P_G is the conductor loss due to the ground planes. To calculate P_G, we first solve for the magnetic field H_x as

$$H_x(\bar{r}) = \sum_{k=1}^{M} \sum_{m=1}^{N_k} \left[\sum_{i=1}^{M} \psi_i a_{km}^{(i)} \right] \int_{\Gamma_{km}} P_{km}(\bar{r}') d\bar{r}' \int_{-\infty}^{\infty} dk_x e^{ik_x(x-x')} \left[-\frac{1}{\mu_0} \frac{\partial \tilde{g}^E(k_x, z, z')}{\partial z} \right] \tag{58}$$

where $\tilde{g}^E(k_x, z, z')$ is the Fourier transform with respect to x of $g^E(\bar{r}, \bar{r}')$ as defined in (37). Thus, we have

$$P_G = 2\pi R_S \sum_{k=1}^{M} \sum_{m=1}^{N_k} \sum_{k'=1}^{M} \sum_{m'=1}^{N_{k'}} \left[\sum_{i=1}^{M} \psi_i a_{km}^{(i)} \right]^* \left[\sum_{i=1}^{M} \psi_i a_{k'm'}^{(i)} \right]$$

$$\int_{\Gamma_{km}} d\bar{r}' P_{km}(\bar{r}') \int_{\Gamma_{k'm'}} d\bar{r}'' P_{k'm'}(\bar{r}'') \int_0^\infty dk_x \cos[k_x(x'-x'')] \left[-\frac{1}{\mu_0}\frac{\partial \tilde{g}^E(k_x, z_G, z')}{\partial z}\right]^* \left[-\frac{1}{\mu_0}\frac{\partial \tilde{g}^E(k_x, z_G, z'')}{\partial z}\right] \tag{59}$$

where R_S is the surface resistance per unit area of the ground planes, z_G is the z coordinate of the ground planes.

Now, set $\overline{\overline{G}} = 0$ in (45b), we have

$$(\alpha_{nC} - i\beta_n)^2 \overline{V}_n = \left[\overline{\overline{R}} - i\omega\overline{\overline{L}}\right] \cdot \left[-i\omega\overline{\overline{C}}\right] \cdot \overline{V}_n \tag{60}$$

Making the approximation that $\beta_n \approx \beta_{0n}$, $\overline{V}_n \approx \overline{V}_{0n}$, and utilizing the relation (44) with $\overline{\overline{G}} = 0$, the imaginary part of (60) becomes

$$2\alpha_{nC} V_{0n,m} = \sum_{k=1}^{M} R_{mk} I_{0n,k}, \qquad 1 \le n, m \le M \tag{61}$$

where $I_{0n,k}$ is the k th element of $\overline{I}_{0n}$; and $V_{0n,m}$ is the m th element of $\overline{V}_{0n}$. The elements of $\overline{\overline{R}}$ can be obtained by solving (61).

After obtaining the matrices $\overline{\overline{C}}$, $\overline{\overline{L}}$, $\overline{\overline{G}}$, and $\overline{\overline{R}}$; the matrix equations (44) and (45) can be solved for the eigenvalues and eigenvectors.

3.6 Transmission Line Analysis

The voltage and current along the transmission lines can be represented in terms of the eigenvectors obtained in the last section as

$$\begin{aligned}\overline{V}(y) &= \sum_{n=1}^{M} a_n \overline{V}_n e^{-\gamma_n y} + \sum_{n=1}^{M} b_n \overline{V}_n e^{\gamma_n y} \\ &= \overline{\overline{S}}_V \cdot \overline{\overline{\Lambda}}(y) \cdot \overline{A} + \overline{\overline{S}}_V \cdot \overline{\overline{\Lambda}}(-y) \cdot \overline{B} \end{aligned} \tag{62a}$$

$$\begin{aligned}\overline{I}(y) &= \sum_{n=1}^{M} a_n \overline{I}_n e^{-\gamma_n y} - \sum_{n=1}^{M} b_n \overline{I}_n e^{\gamma_n y} \\ &= \overline{\overline{S}}_I \cdot \overline{\overline{\Lambda}}(y) \cdot \overline{A} - \overline{\overline{S}}_I \cdot \overline{\overline{\Lambda}}(-y) \cdot \overline{B} \end{aligned} \tag{62b}$$

where $\overline{\overline{S}}_V$ is the matrix with the eigenvector $\overline{V}_n$ as its n th column; $\overline{\overline{S}}_I$ is the matrix with the eigenvector $\overline{I}_n$ as its n th column; $\overline{A}$ and $\overline{B}$ are the mode coefficient vectors in the forward and backward directions, respectively; $\overline{\overline{\Lambda}}(y)$ is a diagonal matrix with $\exp(-\gamma_n y)$ as its n th element; namely,

$$\overline{A} = (a_1, a_2, \cdots, a_M)^T \tag{63a}$$

$$\overline{B} = (b_1, b_2, \cdots, b_M)^T \tag{63b}$$

$$\overline{\overline{\Lambda}}(y) = \text{diag.}\left\{e^{-\gamma_1 y}, e^{-\gamma_2 y}, \cdots, e^{-\gamma_M y}\right\} \tag{63c}$$

where the superscript T represents the transpose of a row vector.

The characteristic impedance matrix can be defined as

$$\overline{\overline{Z}}_C = \overline{\overline{S}}_V \cdot \overline{\overline{S}}_I^{-1} \tag{64}$$

From (62), the mode coefficients $\overline{A}$ and $\overline{B}$ can be represented in terms of the line voltages $\overline{V}(0)$ and line currents $\overline{I}(0)$ as

$$\overline{A} = \frac{1}{2}\left[\overline{\overline{S}}_V^{-1} \cdot \overline{V}(0) + \overline{\overline{S}}_I^{-1} \cdot \overline{I}(0)\right] \tag{65a}$$

$$\overline{B} = \frac{1}{2}\left[\overline{\overline{S}}_V^{-1} \cdot \overline{V}(0) - \overline{\overline{S}}_I^{-1} \cdot \overline{I}(0)\right] \tag{65b}$$

Next, the line voltages $\overline{V}(l)$ and the line currents $\overline{I}(l)$ can be expressed in terms of $\overline{V}(0)$ and $\overline{I}(0)$ through (65) as

$$\begin{bmatrix} \overline{V}(l) \\ \overline{I}(l) \end{bmatrix} = \begin{bmatrix} \overline{\overline{A}}_{VV}(l) & \overline{\overline{A}}_{VI}(l) \\ \overline{\overline{A}}_{IV}(l) & \overline{\overline{A}}_{II}(l) \end{bmatrix} \cdot \begin{bmatrix} \overline{V}(0) \\ \overline{I}(0) \end{bmatrix} = \overline{\overline{A}}(l) \cdot \begin{bmatrix} \overline{V}(0) \\ \overline{I}(0) \end{bmatrix} \tag{66}$$

where $\overline{\overline{A}}(l)$ is called the transfer matrix for the uniform transmission lines of length l; and the explicit form of the submatrices of $\overline{\overline{A}}(l)$ are

$$\overline{\overline{A}}_{VV}(l) = \frac{1}{2}\overline{\overline{S}}_V \cdot \left[\overline{\overline{\Lambda}}(l) + \overline{\overline{\Lambda}}(-l)\right] \cdot \overline{\overline{S}}_V^{-1} \tag{67a}$$

$$\overline{\overline{A}}_{VI}(l) = \frac{1}{2}\overline{\overline{S}}_V \cdot \left[\overline{\overline{\Lambda}}(l) - \overline{\overline{\Lambda}}(-l)\right] \cdot \overline{\overline{S}}_I^{-1} \tag{67b}$$

$$\overline{\overline{A}}_{IV}(l) = \frac{1}{2}\overline{\overline{S}}_I \cdot \left[\overline{\overline{\Lambda}}(l) - \overline{\overline{\Lambda}}(-l)\right] \cdot \overline{\overline{S}}_V^{-1} \tag{67c}$$

$$\overline{\overline{A}}_{II}(l) = \frac{1}{2}\overline{\overline{S}}_I \cdot \left[\overline{\overline{\Lambda}}(l) + \overline{\overline{\Lambda}}(-l)\right] \cdot \overline{\overline{S}}_I^{-1} \tag{67d}$$

If more than one transmission line section with different characteristics are cascaded, the transfer matrix of each section is multiplied to obtain the overall transfer matrix.

Imposing a voltage source $\overline{V}_S$ in series with an impedance matrix $\overline{\overline{Z}}_S$ at $y = 0$, and imposing a voltage source $\overline{V}_L$ in series with an impedance matrix $\overline{\overline{Z}}_L$ at $y = l$, we have

$$\overline{V}(0) = \overline{V}_S - \overline{\overline{Z}}_S \cdot \overline{I}(0) \tag{68a}$$

$$\overline{V}(l) = \overline{V}_L + \overline{\overline{Z}}_L \cdot \overline{I}(l) \tag{68b}$$

The line voltages at all ports can thus be calculated as

$$\begin{bmatrix} \overline{\overline{I}} & \overline{\overline{A}}_{VI}(l) \cdot \overline{\overline{Z}}_S^{-1} - \overline{\overline{A}}_{VV}(l) \\ \overline{\overline{Z}}_L^{-1} & \overline{\overline{A}}_{II}(l) \cdot \overline{\overline{Z}}_S^{-1} - \overline{\overline{A}}_{IV}(l) \end{bmatrix} \cdot \begin{bmatrix} \overline{V}(l) \\ \overline{V}(0) \end{bmatrix} = \begin{bmatrix} \overline{\overline{A}}_{VI}(l) \cdot \overline{\overline{Z}}_S^{-1} \cdot \overline{V}_S \\ \overline{\overline{A}}_{II}(l) \cdot \overline{\overline{Z}}_S^{-1} \cdot \overline{V}_S + \overline{\overline{Z}}_L^{-1} \cdot \overline{V}_L \end{bmatrix} \tag{69}$$

The transient response can be obtained by using Fourier transform.

For the case of a single microstrip line, we first solve for the capacitance and the inductance per unit length C and L, respectively. Next, solving the eigenvalue equations in the lossless medium, we have

$$\gamma^2 = -\beta^2 = -\omega^2 LC \tag{70a}$$

$$I_0 = 1 \tag{70b}$$

$$V_0 = \sqrt{L/C} \tag{70c}$$

The magnetic flux linkage is $\psi = LI_0 = L$, the time-average power is $P_T = (1/2)\sqrt{L/C}$; and the conductor loss per unit length can be calculated by (57) and (59), hence we have $\alpha_C = P_C/2P_T$. Using (61), we have $R = 2\alpha_C\sqrt{L/C}$. The conductance per unit length can be calculated by using (50). With L, C, R, and G, the eigenvalue and the eigenvector can be solved from (44) and (45) as

$$\gamma = \sqrt{(G - i\omega C)(R - i\omega L)} \tag{71a}$$

$$I = 1 \tag{71b}$$

$$V = Z_C I = \sqrt{\frac{R - i\omega L}{G - i\omega C}} \tag{71c}$$

The transfer matrix $\overline{\overline{A}}(l)$ for a transmission line of length l can be obtained from (67) as

$$\overline{\overline{A}}(l) = \begin{bmatrix} \cosh \gamma l & -Z_C \sinh \gamma l \\ -Z_C^{-1} \sinh \gamma l & \cosh \gamma l \end{bmatrix} \tag{72}$$

For the case of two symmetric microstrip lines, we first solve the eigenvalue equations in the lossless medium for the even and the odd modes, respectively. Thus we have

$$\gamma_e^2 = -\beta_e^2 = -\omega^2 (L_{11} + L_{12})(C_{11} + C_{12}) \tag{73a}$$

$$\overline{I}_{e0} = \begin{bmatrix} 1 \\ 1 \end{bmatrix}, \overline{V}_{e0} = \sqrt{\frac{L_{11} + L_{12}}{C_{11} + C_{12}}} \begin{bmatrix} 1 \\ 1 \end{bmatrix} = \sqrt{\frac{L_{11} + L_{12}}{C_{11} + C_{12}}}\, \overline{I}_{e0} \tag{73b}$$

$$\gamma_o^2 = -\beta_o^2 = -\omega^2 (L_{11} - L_{12})(C_{11} - C_{12}) \tag{73c}$$

$$\overline{I}_{o0} = \begin{bmatrix} 1 \\ -1 \end{bmatrix}, \overline{V}_{o0} = \sqrt{\frac{L_{11} - L_{12}}{C_{11} - C_{12}}} \begin{bmatrix} 1 \\ -1 \end{bmatrix} = \sqrt{\frac{L_{11} - L_{12}}{C_{11} - C_{12}}}\, \overline{I}_{o0} \tag{73d}$$

The magnetic flux linkage and the time-average power can be calculated as

$$\overline{\psi}_e = \overline{\overline{L}} \cdot \overline{I}_{e0} = (L_{11} + L_{12}) \overline{I}_{e0} \tag{74a}$$

$$P_{eT} = \sqrt{\frac{L_{11} + L_{12}}{C_{11} + C_{12}}} \tag{74b}$$

$$\overline{\psi}_o = \overline{\overline{L}} \cdot \overline{I}_{o0} = (L_{11} - L_{12}) \overline{I}_{o0} \tag{74c}$$

$$P_{oT} = \sqrt{\frac{L_{11} - L_{12}}{C_{11} - C_{12}}} \tag{74d}$$

The conductor loss per unit length can be obtained by using (57) and (59), thus we have

$$\alpha_{eC} = P_{eC}/2P_{eT}, \qquad \alpha_{oC} = P_{oC}/2P_{oT} \tag{75}$$

The resistance matrix can be solved from (61) as

$$R_{11} = \alpha_{eC} \sqrt{\frac{L_{11} + L_{12}}{C_{11} + C_{12}}} + \alpha_{oC} \sqrt{\frac{L_{11} - L_{12}}{C_{11} - C_{12}}} \tag{76a}$$

$$R_{12} = \alpha_{eC} \sqrt{\frac{L_{11} + L_{12}}{C_{11} + C_{12}}} - \alpha_{oC} \sqrt{\frac{L_{11} - L_{12}}{C_{11} - C_{12}}} \tag{76b}$$

The conductance matrix per unit length can be calculated by using (50). Substituting these $\overline{\overline{L}}$, $\overline{\overline{C}}$, $\overline{\overline{R}}$, and $\overline{\overline{G}}$ into (44) and (45), we obtain the eigenvalues and eigenvectors for the even and the odd modes as

$$\gamma_e^2 = (y_{11} + y_{12})(z_{11} + z_{12}) \tag{77a}$$

$$\overline{I}_e = \begin{bmatrix} 1 \\ \\ 1 \end{bmatrix}, \qquad \overline{V}_e = Z_e \overline{I}_e \tag{77b}$$

$$\gamma_o^2 = (y_{11} - y_{12})(z_{11} - z_{12}) \tag{77c}$$

$$\overline{I}_o = \begin{bmatrix} 1 \\ \\ -1 \end{bmatrix}, \qquad \overline{V}_o = Z_o \overline{I}_o \tag{77d}$$

where

$$Z_e = \sqrt{\frac{z_{11} + z_{12}}{y_{11} + y_{12}}}, \qquad Z_o = \sqrt{\frac{z_{11} - z_{12}}{y_{11} - y_{12}}} \tag{78}$$

$$\begin{aligned} y_{11} &= G_{11} - i\omega C_{11}, & y_{12} &= G_{12} - i\omega C_{12} \\ z_{11} &= R_{11} - i\omega L_{11}, & z_{12} &= R_{12} - i\omega L_{12}. \end{aligned} \tag{79}$$

The characteristic impedance matrix can be obtained from (64) as

$$\overline{\overline{Z}}_C = \overline{\overline{S}}_V \cdot \overline{\overline{S}}_I^{-1} = \begin{bmatrix} (Z_e + Z_o)/2 & (Z_e - Z_o)/2 \\ \\ (Z_e - Z_0)/2 & (Z_e + Z_o)/2 \end{bmatrix} \tag{80}$$

The transfer matrix of length l can be calculated from (67) as

$$\overline{\overline{A}}_{VV}(l) = \frac{1}{2} \begin{bmatrix} \cosh \gamma_e l + \cosh \gamma_o l & \cosh \gamma_e l - \cosh \gamma_o l \\ \\ \cosh \gamma_e l - \cosh \gamma_o l & \cosh \gamma_e l + \cosh \gamma_o l \end{bmatrix} \tag{81a}$$

$$\overline{\overline{A}}_{VI}(l) = \frac{1}{2} \begin{bmatrix} -Z_e \sinh \gamma_e l - Z_o \sinh \gamma_o l & -Z_e \sinh \gamma_e l + Z_o \sinh \gamma_o l \\ \\ -Z_e \sinh \gamma_e l + Z_o \sinh \gamma_o l & -Z_e \sinh \gamma_e l - Z_o \sinh \gamma_o l \end{bmatrix} \tag{81b}$$

$$\overline{\overline{A}}_{VI}(l) = \frac{1}{2} \begin{bmatrix} -Z_e^{-1}\sinh\gamma_e l - Z_o^{-1}\sinh\gamma_o l & -Z_e^{-1}\sinh\gamma_e l + Z_o^{-1}\sinh\gamma_o l \\ -Z_e^{-1}\sinh\gamma_e l + Z_o^{-1}\sinh\gamma_o l & -Z_e^{-1}\sinh\gamma_e l - Z_o^{-1}\sinh\gamma_o l \end{bmatrix} \tag{81c}$$

$$\overline{\overline{A}}_{II}(l) = \frac{1}{2} \begin{bmatrix} \cosh\gamma_e l + \cosh\gamma_o l & \cosh\gamma_e l - \cosh\gamma_o l \\ \cosh\gamma_e l - \cosh\gamma_o l & \cosh\gamma_e l + \cosh\gamma_o l \end{bmatrix} \tag{81d}$$

In the next section, we demonstrate how the transfer matrix is applied to solve the coupled transmission line problems.

3.7 Results and Discussions

First, we check the results of our method in calculating the capacitance matrix using the spectral domain Green's function and compare it with other methods using the spatial domain Green's function. In Tables 3.1 to 3.4, we present the results of capacitance matrix for different microstrip line configurations. In Table 3.1, the difference between our results and those in [9] is about 1% for the self-capacitance, and is about 0.03% for the mutual capacitance. The difference from those in [10] is about 0.1% for the self-capacitance, and about 1% for the mutual capacitance.

In Table 3.2, the difference between our results and those in [9] is less than 0.7% for the self-capacitance, and is less than 4% for the mutual capacitance. The difference between our results and those in [10] is about 0.01% for the self-capacitance, and is less than 0.4% for the mutual capacitance.

The capacitance matrix for two microstrip lines embedded in the same and different layers of a two-layered medium are presented in Tables 3.3 and 4, respectively. The difference between our results and those in [9] is about 3% for the self-capacitance and about 1% for the mutual capacitance.

In Fig. 3.5, we present the charge distributions on the broad sides of a microstrip line with $t/h = 0.02$ and $w/h = 0.1, 1.0, 2.0$. We use 24 pulses on each broad side, and 2 pulses on each narrow side. It is observed that the charge density on the bottom side of the microstrip

Comparison of Capacitance Matrix Elements (F/m).			
element	present work	[9]	[10]
C_{11}	0.6301×10^{-10}	0.6233×10^{-10}	0.6307×10^{-10}
C_{12}	-0.5929×10^{-11}	-0.5931×10^{-11}	-0.5866×10^{-11}
C_{22}	0.6301×10^{-10}	0.6233×10^{-10}	0.6307×10^{-10}

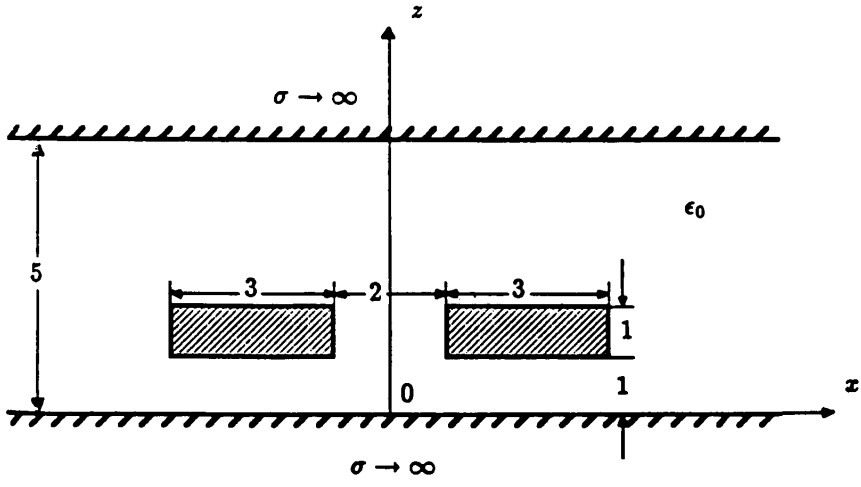

Table 3.1 Comparison of capacitance matrix for two symmetrical striplines of finite thickness.

is about an order larger than that on the top side because the electric field between the microstrip and the ground plane is stronger than the electric field above the microstrip. Also, as the width of the microstrip increases, the edge effect becomes less significant.

In Table 3.5, we present the results of resistance calculation for a microstrip line compared with those in [12]. The discrepancy is 7.6% for $w/h = 0.1$, and 3.4% for $w/h = 2.0$. The calculation of the resistance depends on the square of the charge density distribution which possesses edge effect as shown in Fig. 3.5. Hence, even when two different methods can predict close capacitance results, it is possible that the resistance results can deviate by a higher percentage.

Next, we present the frequency response and the transient response

Comparison of Capacitance Matrix Elements (F/m).			
element	present work	[9]	[10]
C_{11}	0.9225×10^{-10}	0.9165×10^{-10}	0.9224×10^{-10}
C_{12}	-0.8539×10^{-11}	-0.8220×10^{-11}	-0.8504×10^{-11}
C_{22}	0.9225×10^{-10}	0.9165×10^{-10}	0.9224×10^{-10}

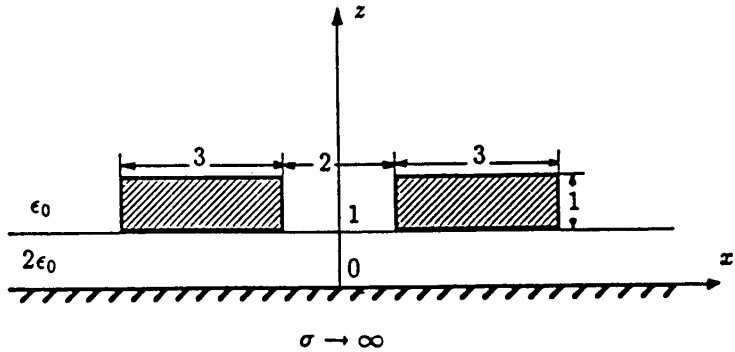

Table 3.2 Comparison of capacitance matrix for two symmetrical microstrip lines of finite thickness.

of two symmetrical microstrip lines. The driving voltage is assumed to have a sinusoidal pulse waveform $V_1(t)$ with duration $\tau = 200$ pico seconds as

$$V_1(t) = \begin{cases} (1/2)[1 - \cos(2\pi t/\tau)], & 0 \le t \le \tau \\ 0, & \text{elsewhere} \end{cases} \tag{82}$$

The frequency response and the transient response are presented in Fig. 3.6(a) and Fig. 3.6(b), respectively, with all the four load impedances equal to the characteristic impedance of the even mode Z_{e0}. In Fig. 3.6(a), $V_1(0)$ is the voltage at $z = 0$ along line 1, $V_1(l)$ is the voltage at the receiving port, $V_2(0)$ is the near-end coupling, and $V_2(l)$ is the far-end coupling. The increase of $V_2(l)$ with frequency shows that the high frequency components are responsible for the far-end coupling[16].

Comparison of Capacitance Matrix Elements (F/m).		
element	present work	[9]
C_{11}	0.3827×10^{-10}	0.3720×10^{-10}
C_{12}	-0.6884×10^{-11}	-0.6889×10^{-11}
C_{22}	0.2245×10^{-10}	0.2169×10^{-10}

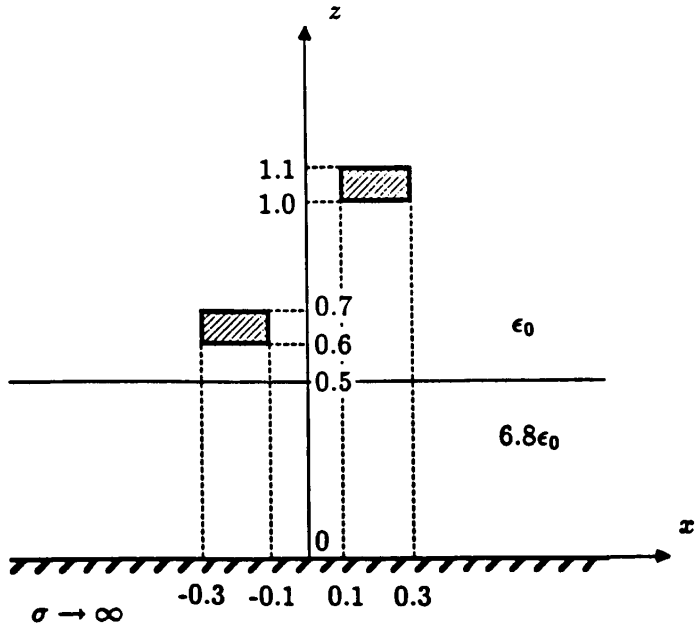

Table 3.3 Comparison of capacitance matrix for two microstrip lines of finite thickness embedded in the same layer of a two-layered medium.

In Fig. 3.6(b), the even and the odd modes propagate in different velocities, and the odd mode propagates faster than the even mode. Hence, the waveform $V_1(l)$ becomes broader than $V_1(0)$, and $V_2(l)$ shows the split of the odd and the even modes. The waveforms $V_1(0)$ and $V_2(0)$ after $t = 800$ ps are due to the reflections by the load impedances at $y = l$. Since the load impedances are chosen to be the same as the characteristic impedance of the even mode, only the odd mode is reflected.

In Fig. 3.7, the transient response is presented with all the four

Comparison of Capacitance Matrix Elements (F/m).		
element	present work	[9]
C_{11}	0.3772×10^{-10}	0.3651×10^{-10}
C_{12}	-0.1583×10^{-11}	-0.1562×10^{-11}
C_{22}	0.2152×10^{-10}	0.2099×10^{-10}

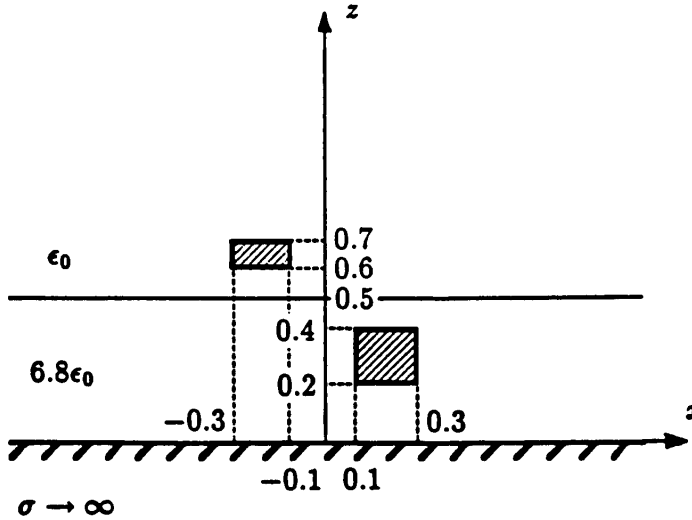

Table 3.4 Comparison of capacitance matrix for two microstrip lines of finite thickness embedded in different layers of a two-layered medium.

load impedances equal to the characteristic impedance of the odd mode Z_{o0}. The split of the odd and the even modes is observed again. The waveforms $V_1(0)$ and $V_2(0)$ after $t = 800$ ps show that only the even mode is reflected, and the reflected signal arrives later than that in Fig. 3.6(b) because the velocity of the even mode is slower than that of the odd mode.

In Fig. 3.8 and Fig. 3.9, we present the transient responses of two symmetrical microstrip lines with $s = 0.25$ mm and $s = 0.375$ mm, respectively. The load impedances are chosen the same as the characteristic impedance of the even mode. Compared with Fig. 3.6(b), it is observed that the coupling signals $V_2(0)$ and $V_2(l)$ become weaker

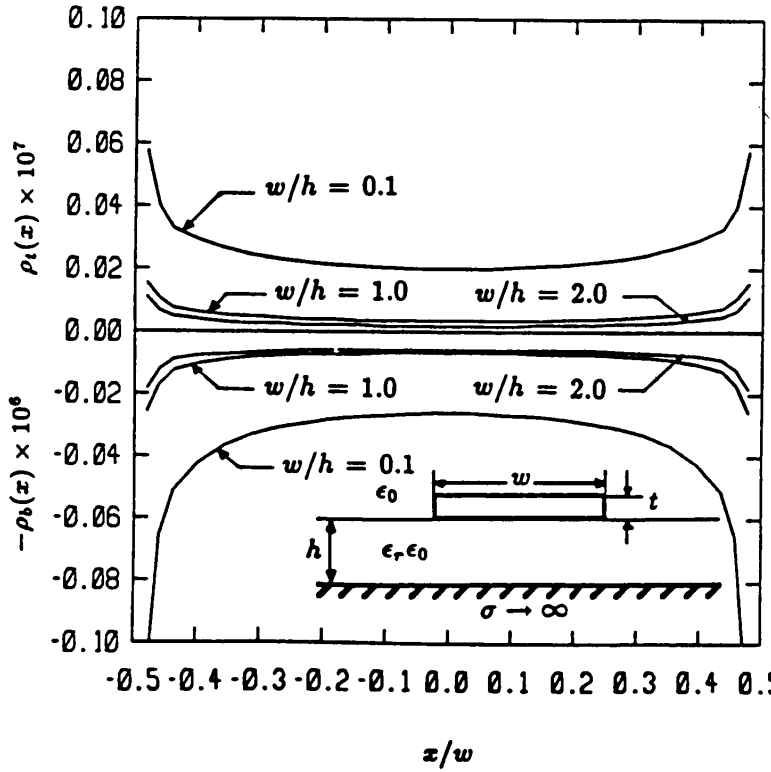

Figure 3.5 The charge distribution on the broad sides of a microstrip line with finite thickness, $\epsilon_r = 11.7$, $h = 2$cm, $t/h = 0.02$, potential on the microstrip surface is 1 volt, 24 pulses per broad side, and 2 pulses per narrow side.

as the separation s is increased.

In Fig. 3.10, the transient responses with a complex dielectric constant $\epsilon_r = 10 + i0.1$ are presented. The signal amplitudes are smaller than those in Fig. 3.6(b) due to the dielectric loss. In Fig. 3.11, the transient responses with copper as the conductor material are presented. The surface resistance is assumed to be $2.61 \times 10^{-7}\sqrt{f}$ ohms. The signal amplitudes are slightly different from those with a perfect conductor because the copper itself is good conductor.

Comparison of Conductor Loss Parameters.				
w/h	$R(\Omega/\mathrm{m})$	$R(\Omega/\mathrm{m})$ [12]	$\alpha Z_0 h/R_s$ (dB)	$\alpha Z_0 h/R_s$ (dB) [12]
0.1	0.07125	0.06605	23.713	21.981
0.2	0.04477	0.03993	14.899	13.289
0.3	0.03398	0.02986	11.309	9.937
0.4	0.02795	0.02400	9.303	8.120
0.6	0.02124	0.01848	7.069	6.150
1.0	0.01492	0.01315	4.967	4.376
1.2	0.01308	0.01173	4.353	3.904
1.4	0.01165	0.01063	3.876	3.538
2.0	0.00872	0.00843	2.901	2.807

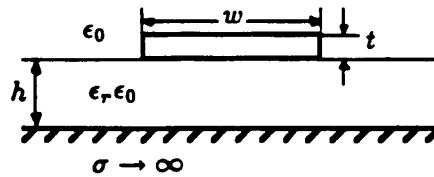

Table 3.5. Comparison of the conductor loss parameters for a microstrip line of finite thickness.

Conclusions

The spectral domain scalar Green's function in a lossy isotropic stratified medium is derived. A rigorous integral equation formulation for the charge distribution on the surfaces of the microstrip lines with finite thickness embedded in arbitrary layers of an isotropic stratified medium is derived. Using the spectral domain Green's function, a multiconductor transmission line analysis is formulated to investigate the propagation properties of coupled lossy microstrip lines. Both the frequency and the transient responses of coupled lines with different load conditions can be obtained. An efficient algorithm is devised based on this approach.

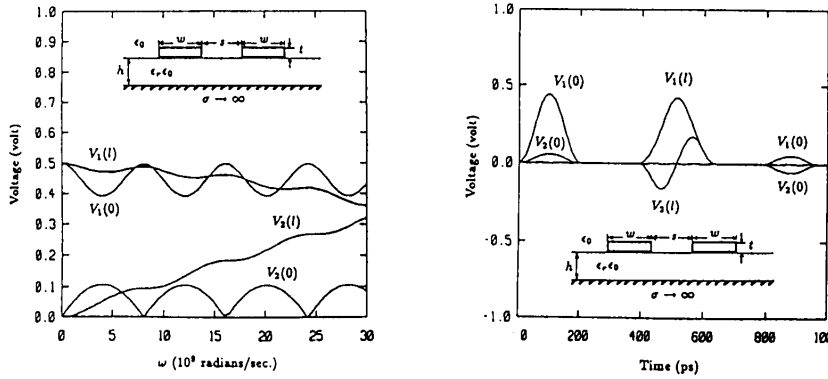

Figure 3.6 Response of two symmetric microstrip lines, $h = 0.2$mm, $w = 0.125$mm, $t = 5\mu$m, $s = 0.125$mm, $l = 5$cm, $\epsilon_r = 10$, all conductors are perfect, $Z_1 = Z_2 = Z_3 = Z_4 = Z_{e0} \approx 72.270\Omega$. (a) Frequency response. (b) Transient response.

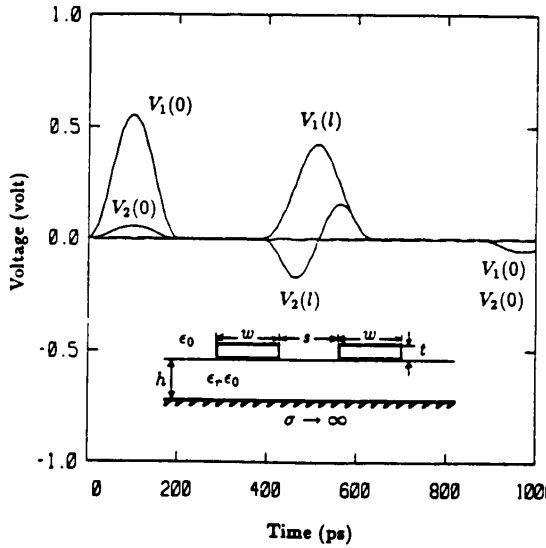

Figure 3.7 Transient response of two symmetric microstrip lines, $h = 0.2$mm, $w = 0.125$mm, $t = 5\mu$m, $s = 0.125$mm, $l = 5$cm, $\epsilon_r = 10$, all conductors are perfect, $Z_1 = Z_2 = Z_3 = Z_4 = Z_{o0} \approx 45.862\Omega$.

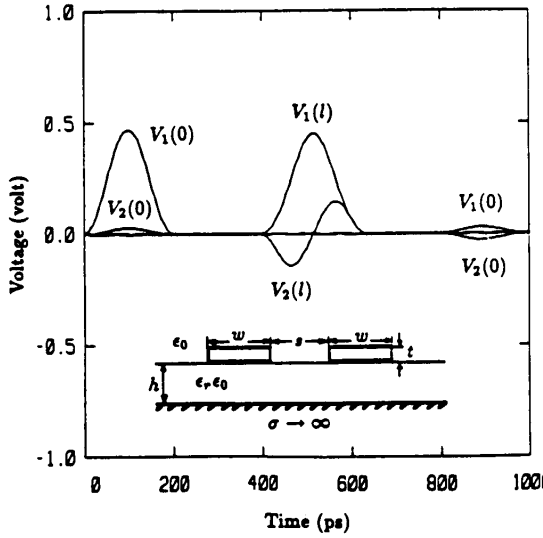

Figure 3.8 Transient response of two symmetric microstrip lines h = 0.2mm, w = 0.125mm, t = 5μm, s = 0.25mm, l = 5cm, ϵ_r = 10, all conductors are perfect, $Z_1 = Z_2 = Z_3 = Z_4 = Z_{e0} \approx 66.345\Omega$.

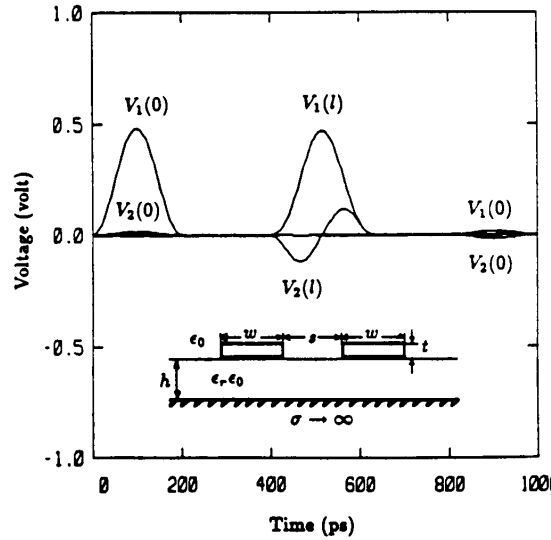

Figure 3.9 Transient response of two symmetric microstrip lines, h = 0.2mm, w = 0.125mm, t = 5μm, s = 0.375mm, l = 5cm, ϵ_r = 10, all conductors are perfect, $Z_1 = Z_2 = Z_3 = Z_4 = Z_{e0} \approx 63.567\Omega$.

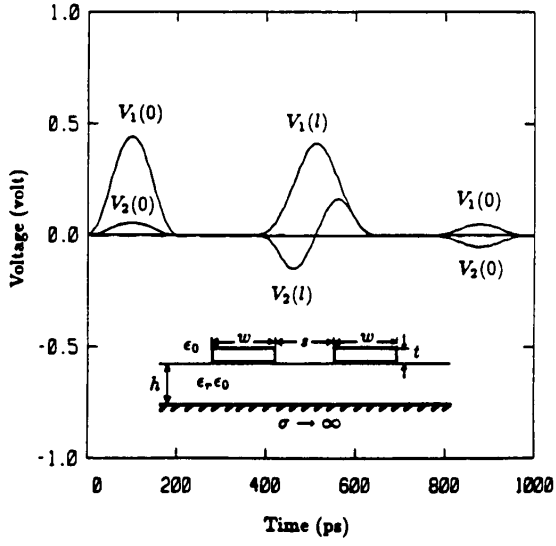

Figure 3.10 Transient response of two symmetric microstrip lines, $h = 0.2$mm, $w = 0.125$mm, $t = 5\mu$m, $s = 0.125$mm, $l = 5$cm, $\epsilon_r = 10 + i0.1$, all conductors are perfect, $Z_1 = Z_2 = Z_3 = Z_4 = Z_{e0} \approx 72.270\Omega$.

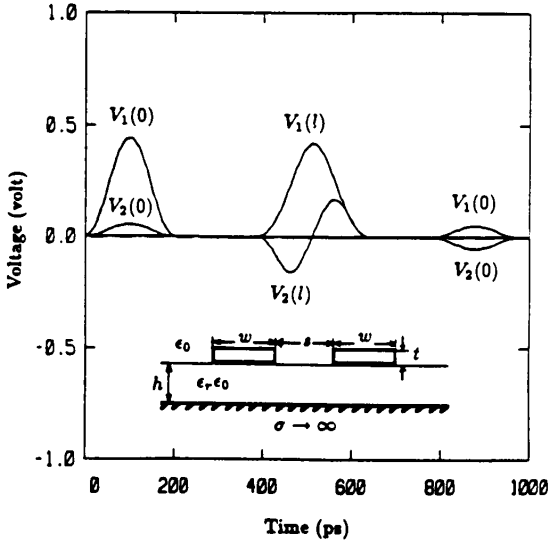

Figure 3.11 Transient response of two symmetric microstrip lines, $h = 0.2$mm, $w = 0.125$mm, $t = 5\mu$m, $s = 0.125$mm, $l = 5$cm, $\epsilon_r = 10$, all conductors are copper, $Z_1 = Z_2 = Z_3 = Z_4 = Z_{e0} \approx 72.270\Omega$.

References

[1] Tripathi, V. K., "Asymmetric coupled transmission lines in an inhomogeneous medium," *IEEE Trans. Microwave Theory Tech.*, **MTT-23**, No. 9, 734–739, September 1975.

[2] Marx, K. D., "Propagation modes, equivalent circuits, and characteristic terminations for multiconductor transmission lines with inhomogeneous dielectrics," *IEEE Trans. Microwave Theory Tech.*, **MTT-21**, 450–457, July 1973.

[3] Djordjevic, A. R., T. K. Sarkar, and R. F. Harrington, "Time-domain response of multiconductor transmission lines," *Proc. IEEE*, No. 6, 743–764, June 1987.

[4] Seki, S. and H. Hasegawa, "Analysis of crosstalk in very high-speed LSI/VLSI's using a coupled multiconductor MIS microstrip line model," *IEEE Trans. Microwave Theory Tech.*, **MTT-32**, No. 12, 1715–1720, December 1984.

[5] Chilo, J. and T. Arnaud, "Coupling effects in the time domain for an interconnecting bus in high-speed GaAs logic circuits," *IEEE Trans. Electron Devices*, **ED–31**, No. 3, 347–352, March 1984.

[6] Yuan, H. T., Y. T. Lin, and S. Y. Chiang, "Properties of interconnection on silicon, sapphire, and semi-insulating gallium arsenide substrates," *IEEE J. Solid-State Circuits*, **SC–17**, No. 2, 269–274, April 1982.

[7] Medina, F. and M. Horno, "Determination of Green's function matrix for multiconductor and anisotropic multidielectric planar transmission lines : a variational approach," *IEEE Trans. Microwave Theory Tech.*, **MTT-33**, No. 10, 933–940, October 1985.

[8] Koul, S. K. and B. Bhat, "Generalized analysis of microstrip-like transmission lines and coplanar strips with anisotropic substrates for MIC, electro-optic modulator, and SAW application," *IEEE Trans. Microwave Theory Tech.*, **MTT-31**, No. 12, 1051–1058, December 1983.

[9] Wei, C., R. F. Harrington, J. R. Mautz, and T. K. Sarkar, "Multiconductor transmission lines in multilayered dielectric media," *IEEE Trans. Microwave Theory Tech.*, **MTT-32**, No. 4, 439–449, April 1984.

[10] Weeks, W. T., "Calculation of coefficients of capacitance of multiconductor transmission lines in the presence of a dielectric interface," *IEEE Trans. Microwave Theory Tech.*, **MTT-18**, No. 1, 35–43, January 1970.

[11] Pucel, R. A., D. J. Masse, and C. P. Hartwig, "Losses in microstrip," *IEEE Trans. Microwave Theory Tech.*, **MTT-16**, No. 6, 342–350, June 1968.

[12] Harrington, R. F. and C. Wei, "Losses on multiconductor transmission lines in multilayered dielectric media," *IEEE Trans. Microwave Theory Tech.*, **MTT-32**, No. 7, 705–710, July 1984.

[13] Syahkal, D. M. and J. B. Davies, "Accurate solution of microstrip and coplanar structures for dispersion and for dielectric and conductor losses," *IEEE Trans. Microwave Theory Tech.*, **MTT-27**, No. 7, 694–699, July 1979.

[14] Kong, J. A., *Electromagnetic Waves Theory*, Wiley–Interscience, New York, 1986.

[15] Ali, S. M., T. M. Habashy, and J. A. Kong, "Dyadic Green's function for anisotropic multilayered media," submitted for publication.

[16] Fukuoka Y., Q. Zhang, D. P. Neikirk, and T. Itoh, "Analysis of multilayer interconnection lines for a high-speed digital integrated circuit," *IEEE Trans. Microwave Theory Tech.*, **MTT-33**, No. 6, 527–532, June 1985.